DOI: 10.1016/j.physb.2014.03.065

Parameterization of the dielectric function of semiconductor nanocrystals

P. Petrik[a,1]

[a] *Institute for Technical Physics and Materials Science (MFA), Research Center for Natural Sciences, Konkoly Thege Rd. 29-33, 1121 Budapest, Hungary*

Abstract

Optical methods like spectroscopic ellipsometry are sensitive to structural properties of semiconductor films such as crystallinity or grain size. The imaginary part of the dielectric function is proportional to the joint density of electronic states. Consequently, the analysis of the dielectric function around the critical point energies provides useful information about the electron band structure and all related parameters like the grain structure, band gap, temperature, composition, phase structure, carrier mobility, etc. In this work an attempt is made to present a selection of the approaches to parameterize and analyze the dielectric function of semiconductors, as well as some applications.

Keywords:
Spectroscopic ellipsometry, Dielectric function, Nanocrystalline semiconductors, Parameterization

1. Introduction

Optical methods, especially polarimetric techniques like ellipsometry, are capable of measuring structural properties of semiconductors [1, 2]. Ellipsometry (and most reflection-based optical methods) can measure nanocrystals in thin layers of optical quality having interfaces that are planar on the scale of several nanometers. The electronic structure of crystalline semiconductors changes strongly with the variation of long range order in the crystal lattice. The imaginary part of the dielectric function measured by ellipsometry is

[1] E-mail://petrik@mfa.kfki.hu, http://petrik.ellipsometry.hu

related to the electronic structure (joint density of states), and it is largely influenced by crystallinity around the critical point energies corresponding to transition energies between parallel bands of the Brillouin zone, revealing high absorption. There is a broad range of material properties that can be determined based on the analysis of the dielectric function, as shown in Fig. 1 [3].

Characteristic critical point energies are 3.4 and 4.2 eV in Si. A spectral range covering these photon energies can easily be measured by standard ellipsometric hardware, usually including the photon energy range of 1.5-5.0 eV and being capable of acquiring accurate and reliable spectra. While the dielectric functions of most single-crystalline semiconductors are available in the literature, the largest problem of measuring non-single-crystalline semiconductors is the requirement of appropriately modeling the dielectric function. There have been numerous approaches like effective medium or oscillator models investigated in the literature used in versatile applications from polycrystalline thin films [4] through ion implanted semiconductors [5, 6] to porous or nanocrystalline structures [7, 8, 9, 10]. There is a trade off between the robustness and the number of fitted parameters used in the optical models. Oscillator models are more accurate, but the large number of fit parameters requires experience, a systematic fitting approach or sophisticated parameter search procedures to avoid getting in local minima.

Another source of error is a possible lateral and vertical inhomogeneity of thin films, which are not taken into account in first order. The most general problem is the vertical non-uniformity, which is characteristic of most deposited thin films. It doesn't only mean a surface and interface roughness or an interface layer of nucleation, but in some cases also a gradual change of properties in the vertical direction, as in most polycrystalline films [11, 12]. A depth scan can be performed by fitting in different wavelength ranges (e.g. for Si the smallest wavelength is fixed at the position for the largest absorption, and the longest wavelength of the range is gradually increased to increase the penetration depth), utilizing the fact that the optical penetration depth changes to a great extent as a function of wavelength around the critical point energies [13].

2. Effective medium methods

Effective medium methods are the most widely used and robust ways to describe the dielectric function of not only semiconductors but any other

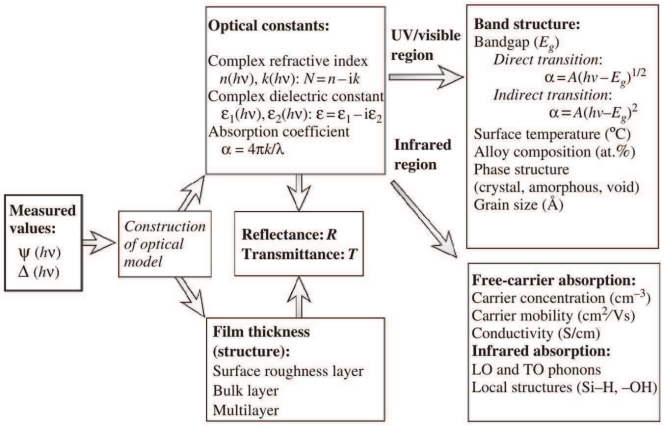

Figure 1: Scheme of an ellipsometric measurement. Optical models are constructed to determine optical properties and layer thicknesses. The reflectance and transmittance is not measured directly, but they can be determined from the optical models using the best-fit parameters. There is a large number of material properties that can be determined from the optical properties. Due to the high sensitivity of ellipsometry to the dielectric function (10^{-3}-10^{-4}), material properties with small influence on the optical properties can also be measured. (Reproduced from Ref. [3].)

composite structures consisting of distinct phases that can be described by their bulk dielectric functions and that are smaller than the wavelength of illumination [4, 14]. The effective dielectric function (ϵ) can be calculated from the dielectric functions of the components ($\epsilon_a, \epsilon_b, ...$) and their volume fractions ($f_a, f_b, ...$) by the equation

$$\frac{\epsilon - \epsilon_h}{\epsilon + 2\epsilon_h} = f_a \frac{\epsilon_a - \epsilon_h}{\epsilon_a + 2\epsilon_h} + f_b \frac{\epsilon_b - \epsilon_h}{\epsilon_b + 2\epsilon_h}, \tag{1}$$

where ϵ_h denotes the dielectric function of the host. If b represents a dilute phase then we can choose $\epsilon_h = \epsilon_a$, which leads to the Maxwell Garnett expression:

$$\frac{\epsilon - \epsilon_a}{\epsilon + 2\epsilon_a} = f_b \frac{\epsilon_b - \epsilon_a}{\epsilon_b + 2\epsilon_a}. \tag{2}$$

If the volume fraction of the components are comparable, it may not be clear, which component whould be the host medium. In this case a self-consistent choice is $\epsilon_h = \epsilon$ resulting in the Bruggeman expression:

$$0 = f_a \frac{\epsilon_a - \epsilon}{\epsilon_a + 2\epsilon} + f_b \frac{\epsilon_b - \epsilon}{\epsilon_b + 2\epsilon}. \tag{3}$$

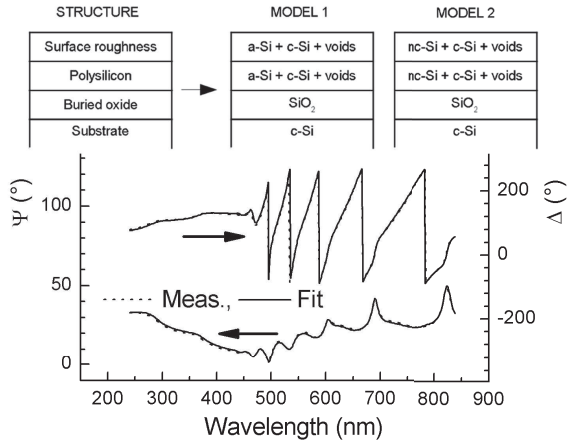

Figure 2: Measured (angle of incidence of 75°) and fitted ellipsometric spectra of a 100-nm polycrystalline Si film deposited on oxidized (100 nm) Si using low pressure chemical vapor deposition at a temperature of 640°C. At the top of the figure the assumed layer structure and two possible optical models depending on the grain structure are shown. In this fit Model 2 has been used.

A typical example of the Bruggeman effective medium theory is the modeling of polycrystalline materials, which can usually be considered as a composition of certain phases like single-crystalline Si (c-Si), amorphous Si (a-Si), fine-grained polycrystalline Si (nc-Si) and voids (vacuum, i.e. a refractive index of $n = 1$) for polycrystalline Si [15, 11, 16], as shown in Fig. 2.

3. Analytical models

If the assumption that the investigated film has distinct phases is not valid, or if there is no reliable reference dielectric function for the components, the effective medium approach fails. Analytical models describe the dielectric function with parameterized functions derived from physical principles like the generalized oscillator model [17], the model dielectric function [18] or the Forouhi-Bloomer model [19], or providing mathematical line shapes such as the Kim-Garland model [20], the Johs-Herzinger model [21] or the B-spline model [22]. While the advantage of the effective medium models is that they describe the optical properties with few parameters and that they allow the determination of volume fractions of known phases, the major advantage of analytical parameterizations is that their fitted parameters can

be related to numerous derived physical properties that are highly relevant in semiconductor technology and materials science (see Fig. 1).

3.1. Lorentz oscillators

A general and usual approach to fit the dielectric function is to use a set of Lorentz oscillators:

$$\epsilon_L(E) = \epsilon_{L,\infty} + \sum_{i=1}^{n} \frac{A_{i,L}^2}{(E_{i,L}^2 - E^2) - i\Gamma_L, E}, \tag{4}$$

where E, A_L, Γ_L and E_L denote the photon energy, the amplitude, the broadening and the oscillator energy, respetcively. This method is often used to have a smooth analytical representation of the dielectric function which allows the accurate determination of peak positions and broadenings [23] or serves as a starting point for further analysis [24]. This method has been extended with Gaussian broadening to achieve a better fit on metal films [25]. It has been shown by numerous investigations that the broadening parameter of the critical point features is proportional to the grain size [24, 9].

If the size of nanocrystal inclusions is so small that the band structure gets close to that of amorphous semiconductors, the Tauc-Lorentz method can be applied [26, 27]. This approach combines (i.e. calculates the convolution of) Lorentz oscillators and the quadratic Tauc gap,

$$\epsilon_{2,T}(E) = \frac{A_T E_{0,T} \Gamma_T (E - E_{g,T})^2}{(E^2 - E_{g,T}^2)^2 + \Gamma_T^2 E^2} \Theta(E - E_{g,T}), \tag{5}$$

where $\Theta(x < 0) = 0$, $\Theta(x \geq 0) = 1$, A_T, Γ_T, $E_{g,T}$ and $E_{0,T}$ are the amplitude, broadening, band gap and the peak energy in the joint density of states, respectively. The corrected expression for the real part of the dielectric function is given in Ref. [28]. The Tauc-Lorentz method has been proven to be useful for modeling amorphous semiconductors. This way a quadratic behavior is assumed at the band edge while the simplicity of the combination of Lorentz oscillators is maintained. In the model a Kramers-Kronig consistent analytical formula is constructed for the real part of the dielectric function. This provides simplicity for the computational adaptation of the model, and at the same time provides a powerful concept, because well-defined numerical information (like the band gap) can be determined for the investigated thin film. This is the reason for the popularity of this model which leads to its application as an empirical model even for non-amorphous materials [29, 30].

The absorption formula of the Tauc-Lorentz model near to the band edge has been refined using the Cody-Lorentz model

$$\epsilon_{2,C}(E) = \frac{E_{1,C}}{E} exp\left(\frac{E - E_{t,C}}{E_{u,C}}\right)\Theta(E_{t,C} - E) + \epsilon_{2,T}\Theta(E - E_{t,C}), \quad (6)$$

where $E_{t,C}$ is the demarcation energy between the exponential Urbach tail transition ($\alpha_C[E] = \alpha_{0,C} exp[E/E_{u,C}]$, with α being the absorption coefficient), $\epsilon_{2,T}$ is the Tauc-Lorentz expression from eq. 5, and $E_{1,C}$ is the amplitude. The Cody-Lorentz method was suggested and the analytical formula for the real part of the dielectric function was derived by Ferlauto and coworkers [31].

3.2. Forouhi-Bloomer model

The Forouhi-Bloomer model [19] derived from quantum mechanical considerations takes the form of

$$n_F(E) = n_F(\infty) + \frac{B_{0,F}E + C_{0,F}}{E^2 - B_F E + C_F}, \quad (7)$$

$$k_F(E) = \frac{A_F(E - E_{g,F})^2}{E^2 - B_F E + C_F}, \quad (8)$$

where

$$B_{0,F} = \frac{A_F}{Q_F}\left(-\frac{B_F^2}{2} + E_{g,F}B_F - E_{g,F}^2 + C_F\right), \quad (9)$$

and

$$C_{0,F} = \frac{A_F}{Q_F}\left((E_{g,F}^2 + C_F)\frac{B_F}{2} - 2E_{g,F}C_F\right), \quad (10)$$

which uses only 5 fit parameters (A_F, B_F, C_F, $E_{g,F}$ and $n_F(\infty)$, $Q_F = 0.5(4C_F - B_F^2)^{1/2}$) for both n_F and k_F in a relatively simple but also Kramers-Kronig consistent way. This method is suited for the description of amorphous semiconductors, which has later been improved by McGahan [32] and Jellison [26].

3.3. Generalized oscillator model

The generalized oscillator model [17] applies a set of oscillators for the critical points described by

$$\epsilon_G(E) = C_G - A_G e^{i\Phi_G}(E - E_{0,G} + i\Gamma_G)^l, \quad (11)$$

where C_G, A_G, Φ_G, $E_{0,G}$, and Γ_G denote the offset, amplitude, phase, threshold energy and broadening, respectively. The exponent l has the value of -0.5 for one-dimensional, 0 for two-dimensional and +0.5 for three-dimensional critical points. Discrete excitons are represented by $l = -1$. The most effective way of applying this method is to fit the derivative of the dielectric function, because this way the effect of surface non-idealities (especially when caused by low-dispersion overlayers) on the line shape of critical point features can be decreased significantly. Besides the determination of the temperature dependence of the critical point features of different semiconductors [33, 17, 34], the generalized oscillator model has also been applied for various semiconductors, e.g. for CdTe [35].

3.4. Model dielectric function

Model dielectric functions have been derived by Adachi for a range of semiconductors from electronic band structure calculations [18, 36]. Kramers-Kronig-consistent expressions have been provided for each critical point. In case of Si, the most characteristic transitions of a two-dimensional M_0-type E_1

$$\epsilon_A(E) = -B_A^{-2} ln(1 - \chi_{1,A}^2) \tag{12}$$

with

$$\chi_{1,A} = \frac{E + i\Gamma_A}{E_{1,A}}, \tag{13}$$

and a two-dimensional M_2-type E_2

$$\epsilon_A(E) = -F_A^{-2} ln \frac{1 - \chi_{cl,A}}{1 - \chi_{2m,A}}, \tag{14}$$

with

$$\chi_{2m,A} = \frac{E + i\Gamma_A}{E_{2,A}}, \chi_{cl,A} = \frac{E + i\Gamma_L}{E_{cl,A}}, \tag{15}$$

are completed with several damped harmonic oscillators (eq. 4) for the E_1 excitonic and the two-dimensional (M_2) E_2 transitions. In eqs. 12 and 14 B_A and F_A denote oscillator amplitudes, Γ_A and Γ_L denote the broadening parameters. The applications of this powerful method range from ion implanted materials [37, 38] to porous Si (see Ref. [9] and Fig. 3).

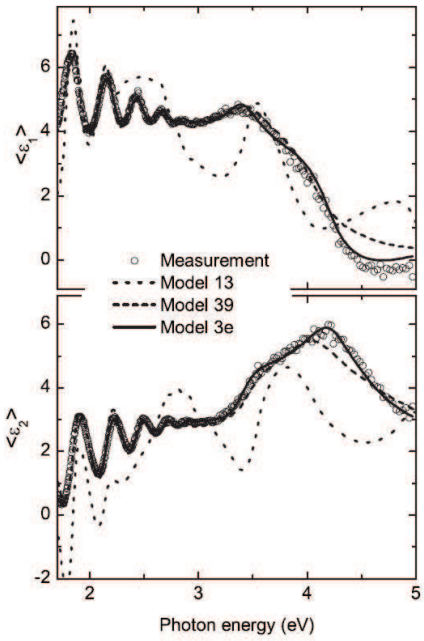

Figure 3: Pseudo dielectric function of a porous Si layer created by anodic etching in bulk single-crystalline Si with a resistivity of 0.03 Ωcm, a nominal thickness of 550 nm and a nominal size of nanocrystals of 6 nm fitted using different optical models. Model "13" denotes a one-layer optical model with 3 fitted parameters: the thickness, the volume fraction of fine-grained polycrystalline Si and voids in an effective medium mixture with single-crystalline Si. Model "39" uses 3 layers with the same components as that of Model "13", whereas Model "3e" stands for the fit using the model dielectric function. (Reproduced from Ref. [9].)

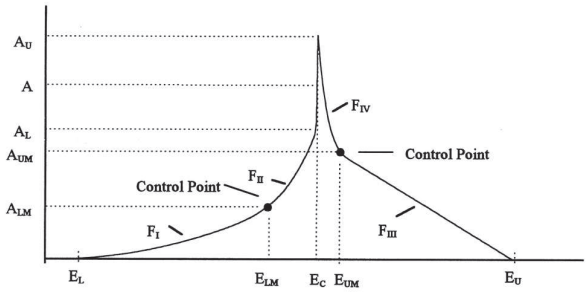

Figure 4: Johs-Herzinger critical point feature composition using four component polynomials [21].

3.5. Polynomial-based models

3.5.1. Kim-Garland model

Kim et al. developed a model which describes the dielectric function around the critical points using polynomials [39, 20]. They have also shown that using a Gaussian broadening allows a significantly better fit also to the derivatives, than using a Lorentzian broadening. The use of this approach has been demonstrated for GaAs [39] as well as for $Al_xGa_{1-x}As$ [20].

3.5.2. Johs-Herzinger generalized critical point model

The Johs-Herzinger generalized critical point model uses the same approach as the Kim-Garlan model, but in an improved way. It has been introduced at the 2nd International Conference on Ellipsometry in 1997 and published in Ref. [21]. It has been demonstrated on the example of fitting the dielectric function of $Hg_{1-x}Cd_xTe$ thin films (Fig. 4). This method utilizes four polynomials to provide a general empirical description of all kinds of critical point features. Finally, a Gaussian broadening is defined for each of them. It results in a large number of fit parameters. Therefore, the use of this method requires much experience and a careful analysis to fix as much parameters as possible at physically reasonable values. The real part of the dielectric function is calculated using look-up tables and therefore the analytic implementation of the model is problematic – it is bound to the proprietary software of the Woollam Co. The applications of this method span a wide range from Si [40, 16] to ZnO [41].

3.5.3. B-spline model

If the layer thicknesses and optical properties in a structure are known except for one layer, the real and imaginary parts of the dielectric function of that unknown layer can be determined by direct numerical inversion at each wavelength independently [42]. The advantage of this method is that no dispersion model is required and fine details of the absorption features can be characterized. However, the dielectric function calculated this way is usually scattered and easily jumps into unphysical results because of the large sensitivity on the correctness of all fixed thicknesses and optical constants, and because of the effect caused by the wavelength dependence of the penetration depth and the vertical inhomogeneity of the investigated layers.

The idea of using splines is connected to the assumption that the dielectric function can be considered smooth in a narrow wavelength range. Then the data in these ranges can be coupled by fitting polynomial spline functions. The method has been suggested and first applied by Zettler et al. [43], which has been developed further by Johs and Hale [22] using B-splines ("B" stands for basis) that has a range of theoretical and practical advantages over simple polynomial splines. Using B-splines, control points can be set arbitrarily, which allow to distinguish between spectral ranges of low and high dispersion.

As an example, the B-spline fit of the dielectric function of Au is shown in Fig. 5. The distance between the nodes were set to 0.2 eV. Increasing this value reduces the number of fitted parameters significantly, but the fine details of the spectrum cannot be followed so accurately as in case of a high node resolution. This parameter can manually be adjusted, and in some cases the model is robust enough to involve the layer thickness as well (as a fit parameter) together with a high-resolution B-spline fit on the dielectric function.

Figure 6 shows an example of fitting a 50-nm ZnO layer (sputtered on a single-crystallin Si substrate) using the B-spline model, the Johs-Herzinger model and the Tauc-Lorenz model [44]. The number of fitted parameters are almost the same for the Johs-Herzinger and the Tauc-Lorentz models (6 and 5 respectively), while the B-spline model uses much more parameters, therefore the measured and fitted curves are almost identical (similar to the case of Fig. 5). The detailes of the analysis will be given in Ref. [44].

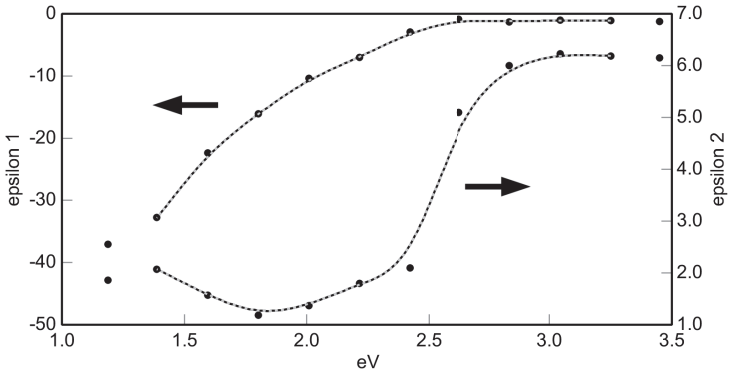

Figure 5: B-spline fit on Au. The dots represent the control points with a resolution of 0.2 eV. The dashed lines show the dielectric functions fitted using the B-splines. The solid gray curves denote the measured spectra from the Woollam database. The measured and fitted spectra are coincident, with differences smaller than the linewidth.

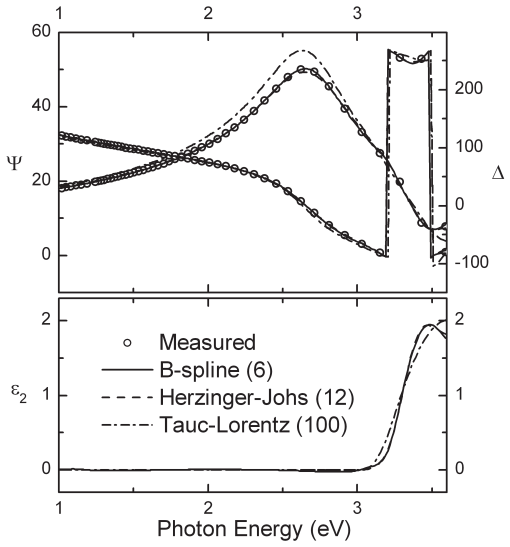

Figure 6: Fitted Ψ and Δ ellipsometric spectra (top graph) and the resulting imaginary part of the dielectric function (ϵ_2 on the bottom graph) using the B-spline, the Johs-Herzinger and the Tauc-Lorentz models on a 50-nm ZnO film deposited on a single-crystalline Si substrate using sputtering. The mean squared errors of the fits are shown in parentheses.

4. Line shape analysis

To determine the band edge features (i.e. band gap energy) a common approach is to analyze the imaginary part of the dielectric function as a function of the photon energy in a range close to the expected band gap. For this approach the dielectric function of the layer has to be determined either by direct numerical inversion from bulk or thin film models, or by fitting the dielectric function with some high resolution empirical models like the B-spline method. In some cases just the pseudo dielectric function is used neglecting the effect of surface and bottom interfaces.

As soon as accurate dielectric function data are determined, the line shape can be fitted by relevant functions, like fitting a quadratic line shape [45] or equivalently, by applying a semi-logarithmic Tauc plot of $\alpha^{1/2} \propto E$ in which the intersection of a linear fit with the photon energy axis provides the band gap [46, 47, 48, 49].

The systematic change of the optical properties can also be investigated by recording the peak positions of the imaginary part of the dielectric function or its derivatives. The analysis of the correlation of this change with certain process parameters can provide insight into the processes or directly enable the determination of key physical parameters of the system.

An interesting application of this concept is a method suggested by Aspnes et al. [50] for the determination of excitation areas induced by energetic ions implanted into GaAs. The assumption is that the tracks of impinging ions are located randomly on the sample surface, so the probability of further amorphization by the next ion is proportional to the remaining crystalline fraction. Consequently, Poisson statistics apply, and the relative decrease in amplitude is $exp(-Fa)$, where F is the fluence and a is the projected size. The application of the method has been demonstrated for different semiconductors including Si, CdTe [51] and SiC [52].

5. Vertical inhomogeneity

Thin films are in most cases non-uniform on the scale of ellipsometric sensitivity in the vertical direction. This doesn't only mean transition and roughness regions at the layer boundaries, but also some vertical gradients of structural and optical properties as can be revealed e.g. in polycrystalline Si [12, 13]. Fig. 7 shows the extinction coefficient (k) of an approximately 500 nm thick deposited polycrystalline silicon layer, and the optical penetration

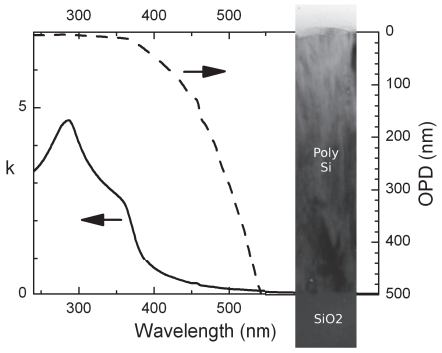

Figure 7: Extinction coefficient (k) of low pressure chemical vapor deposited polycrystalline silicon as a function of the wavelength. The optical penetration depth is also plotted, calculated by OPD=$\lambda/(4\pi k)$. A transmission electron microscopy image of the polycrystalline silicon layer is shown on the right-hand side.

depth calculated directly from k. At the wavelength corresponding to the peak of k ($\sim$300 nm) the penetration depth is approximately 5 nm, and the bottom interface is visible only for wavelengths above $\sim$550 nm. The penetration depth increases rapidly when increasing the wavelength from 300 nm to 500 nm. Consequently, the structure seen by the illuminating light will be different depending on the wavelength (optical properties integrated over different depths). In each case, a vertically changing structure is integrated over the layer thickness or down to the penetration depth depending on the wavelength.

The wavelength dependent penetration depth is an important issue which should be kept in mind especially for polycrystalline semiconductors, for which both the dispersion and the vertical non-uniformity is large. The wavelength dependent penetration depth is not just a disturbing effect, but it can be used for a depth scan when systematically investigating the fitted model parameters as a function of the wavelength range [41].

Conclusions

In this article an attempt was made to summarize some of the methods known for the author that have been successfully used for the parameterization of the dielectric function of semiconductor nanocrystals. There is no method that can be selected as the best for all applications. The success of parameterization depends on the choice of most suitable method with the

least possible parameters. A proper approach is most probably to start with most robust models which use the lowest number of fit parameters, and to refine the model with more sophisticated approaches using some of the parameters determined from the previous approaches as starting parameters or to help to define reasonable ranges for the parameter search. If none of the parameterizations result in an acceptable fit, the B-spline model or the direct numerical inversion could be the best choice, however these can also lead to non-physical results if the layer is inhomogeneous, anisotropic or depolarizing. These effects can be checked when using rotating compensator or generalized Muller matrix ellipsometry.

Acknowledgements

This work was supported by the grants of OTKA K81842 and ENIAC E450EDL.

References

References

[1] P. Petrik, in: S. Neralla (Ed.), Nanocrystals - Synthesis, Characterization and Applications, Intech, Rijeka, 2012.

[2] P. Petrik, M. Fried, in: M. Losurdo, K. Hingerl (Eds.), Ellipsometry at the Nanoscale, Springer-Verlag, Heidelberg, 2012.

[3] H. Fujiwara, J. Koh, C. R. Wronski, R. W. Collins, Appl. Phys. Lett. 70 (1997) 2150.

[4] D. E. Aspnes, Thin Solid Films 89 (1982) 249.

[5] M. Fried, T. Lohner, E. Jároli, C. Hajdu, J. Gyulai, Nucl. Instr. Meth. B 55 (1991) 257.

[6] M. Fried, T. Lohner, W. A. M. Aarnink, L. J. Hanekamp, A. van Silfhout, J. Appl. Phys. 71 (1992) 2835.

[7] M. Fried, T. Lohner, O. Polgar, P. Petrik, E. Vazsonyi, I. Barsony, J. P. Piel, J. L. Stehle, Thin Solid Films 276 (1996) 223.

[8] T. Lohner, N. Q. Khánh, Z. Zolnai, Acta Physica Slovaca 48(4) (1998) 441.

[9] P. Petrik, M. Fried, E. Vazsonyi, P. Basa, T. Lohner, P. Kozma, Z. Makkai, J. Appl. Phys. 105 (2009) 024908.

[10] E. Vazsonyi, E. Szilagyi, P. Petrik, Z. E. Horvath, T. Lohner, M. Fried, G. Jalsovszky, Thin Solid Films 388 (2001) 295.

[11] P. Petrik, M. Fried, T. Lohner, R. Berger, L. P. Biró, C. Schneider, J. Gyulai, H. Ryssel, Thin Solid Films 313-314 (1998) 259.

[12] P. Petrik, T. Lohner, M. Fried, L. P. Biró, N. Q. Khánh, J. Gyulai, W. Lehnert, C. Schneider, H. Ryssel, J. Appl. Phys. 87 (2000) 1734.

[13] P. Petrik, E. Agocs, J. Volk, I. Lukacs, B. Fodor, P. Kozma, T. Lohner, S. Oh, Y. Wakayama, T. Nagata, M. Fried, Thin Solid Films (2014) accepted for publication.

[14] P. Petrik, M. Fried, E. Vazsonyi, T. Lohner, E. Horvath, O. Polgar, P. Basa, I. Barsony, J. Gyulai, Appl. Surf. Sci. 253 (2006) 200.

[15] B. G. Bagley, D. E. Aspnes, A. C. Adams, C. J. Mogab, Appl. Phys. Lett. 38 (1981) 56.

[16] E. Agocs, P. Petrik, S. Milita, L. Vanzetti, S. Gardelis, A. G. Nassiopoulou, G. Pucker, R. Balboni, M. Fried, Thin Solid Films 519 (2011) 3002.

[17] P. Lautenschlager, M. Garriga, L. Vina, M. Cardona, Phys. Rev. B 36 (1987) 4821.

[18] S. Adachi, Phys. Rev. B 35 (1987) 7454.

[19] A. R. Forouhi, I. Bloomer, Phys. Rev. B 34 (1986) 225.

[20] C. C. Kim, J. W. Garland, P. M. Raccah, Phys. Rev. B 47 (1993) 1876.

[21] B. Johs, C. M. Herzinger, J. H. Dinan, A. Cornfeld, J. D. Benson, Thin Solid Films 313 (1998) 137.

[22] B. Johs, J. S. Hale, Phys. Stat. Sol. 205 (2008) 715.

[23] D. E. Aspnes, S. M. Kelso, R. A. Logan, R. Bhat, J. Appl. Phys. 60 (1986) 755.

[24] G. F. Feng, R. Zallen, Physical Review B 40 (1989) 1064.

[25] A. D. Rakic, A. B. Djurisic, J. M. Elazar, M. L. Majewski, Applied Optics 37 (1998) 5271.

[26] G. E. Jellison, Jr., F. A. Modine, Appl. Phys. Lett. 69 (1996) 371.

[27] G. E. Jellison, Jr., V. I. Merkulov, A. A. Puretzky, D. B. Geohegan, G. Eresa, D. H. Lowndes, J. B. Caughman, Thin Solid Films 377-378 (2000) 68.

[28] G. Jellison, Jr., F. Modine, Appl. Phys. Lett. 69 (1996) 2137.

[29] A. C. Galca, M. Secu, A. Vlad, J. D. Pedarnig, Thin Solid Films 518 (2010) 4603.

[30] A. C. Galca, G. Socol, V. Craciun, Thin Solid Films 520 (2012) 4722.

[31] A. S. Ferlauto, G. M. Ferreira, J. M. Pearce, C. R. Wronski, R. W. Collins, Journal of Applied Physics 92 (2002) 2424.

[32] W. A. McGahan, T. Makovicka, J. Hale, J. A. Woollam, Thin Solid Films 253 (1994) 57.

[33] P. Lautenschlager, P. B. Allen, M. Cardona, Phys. Rev. B 31 (1985) 2163.

[34] P. Lautenschlager, M. Garriga, S. Logothetidis, M. Cardona, Phys. Rev. B 35 (1987) 9174.

[35] J. Li, J. Chen, R. W. Collins, Appl. Phys. Lett. 97 (2010) 181909.

[36] S. Adachi, Phys. Rev. B 38 (1988) 12966.

[37] K. Tsunoda, S. Adachi, M. Takahashi, J. Appl. Phys. 91 (2002) 2936.

[38] P. Petrik, M. Fried, T. Lohner, N. Q. Khánh, P. Basa, O. Polgar, C. Major, J. Gyulai, F. Cayrel, D. Alquier, Nucl. Instr. and Meth. B 253 (2006) 192.

[39] C. C. Kim, J. W. Garland, H. Abad, P. M. Raccah, Phys. Rev. B 45 (1992) 11749.

[40] P. Petrik, S. Milita, G. Pucker, A. G. Nassiopoulou, J. A. van den Berg, M. A. Reading, M. Fried, T. Lohner, M. Theodoropoulou, S. Gardelis, M. Barozzi, M. Ghulinyan, A. Luic, L. Vanzetti, A. Picciotto, ECS Transaction 25 (2009) 373.

[41] P. Petrik, B. Pollakowski, S. Zakel, T. Gumprecht, B. Beckhoff, M. Lemberger, Z. Labadi, Z. Baji, M. Jank, A. Nutsch, Appl. Surf. Sci. 281 (2013) 123.

[42] R. W. Collins, A. S. Ferlauto, in: E. G. Irene, H. G. Tomkins (Eds.), Handbook of ellipsometry, William Andrew, Norwich, NY, 2005.

[43] J.-T. Zettler, T. Trepk, L. Spanos, Y.-Z. Hu, W. Richter, Thin Solid Films 234 (1993) 402.

[44] E. Agocs, B. Fodor, B. Pollakowski, B. Beckhoff, A. Nutsch, M. Jank, P. Petrik, Thin Solid Films (2014) to be published.

[45] H. V. Nguyen, R. W. Collins, Phys. Rev. B 47 (1993) 1911.

[46] S. Furukawa, T. Miyasato, Phys. Rev. B 38 (1988) 5726.

[47] H. V. Nguyen, Y. Lu, S. Kim, M. Wakagi, R. W. Collins, Phys. Rev. Lett. 74 (1995) 1995.

[48] L. Miao, P. Jin, K. Kaneko, A. Terai, N. Nabatova-Gabain, S. Tanemura, Appl. Surf. Sci. 212 (2003) 255.

[49] R. K. Gupta, M. Cavas, F. Yakuphanoglu, Spectrochimica Acta Part A: Molecular and Biomolecular Spectroscopy 95 (2012) 107.

[50] D. E. Aspnes, S. Kelso, C. Olson, D. Lynch, Phys. Rev. Lett. 48 (1982) 1863.

[51] P. Petrik, N. Q. Khánh, J. Li, J. Chen, R. Collins, M. Fried, G. Radnoczi, T. Lohner, J. Gyula, Phys. Stat. Sol. (c) 5 (2008) 1358.

[52] P. Petrik, Z. Zolnai, O. Polgar, M. Fried, Z. Betyak, E. Agocs, T. Lohner, C. Werner, M. Röppischer, C. Cobet, Thin Solid Films 519 (2011) 2791.

Figure

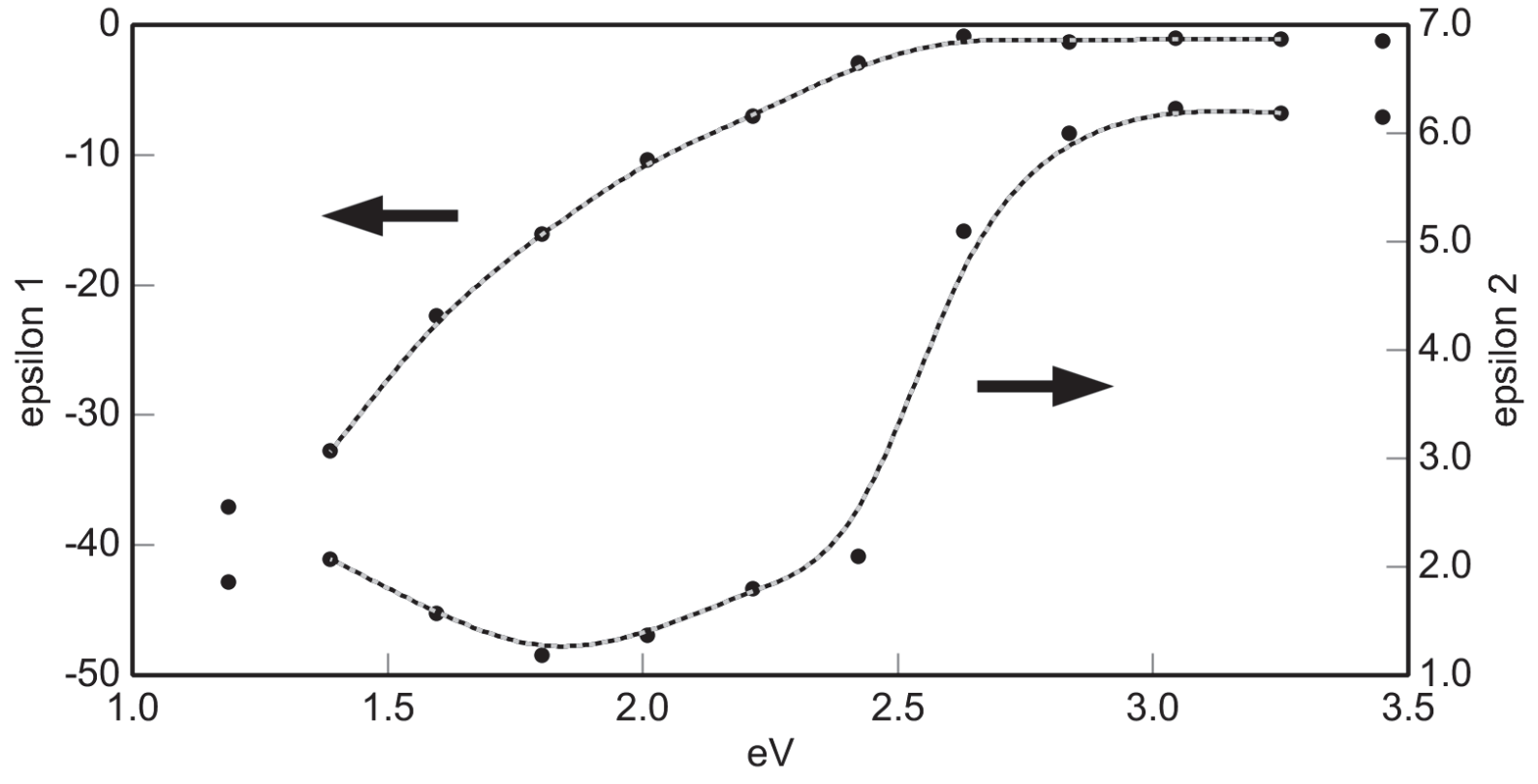
0
-10
-20
-30
-40
-50
epsilon 1
7.0
6.0
5.0
4.0
3.0
2.0
1.0
epsilon 2
1.0
1.5
2.0
2.5
3.0
3.5
eV

Figure

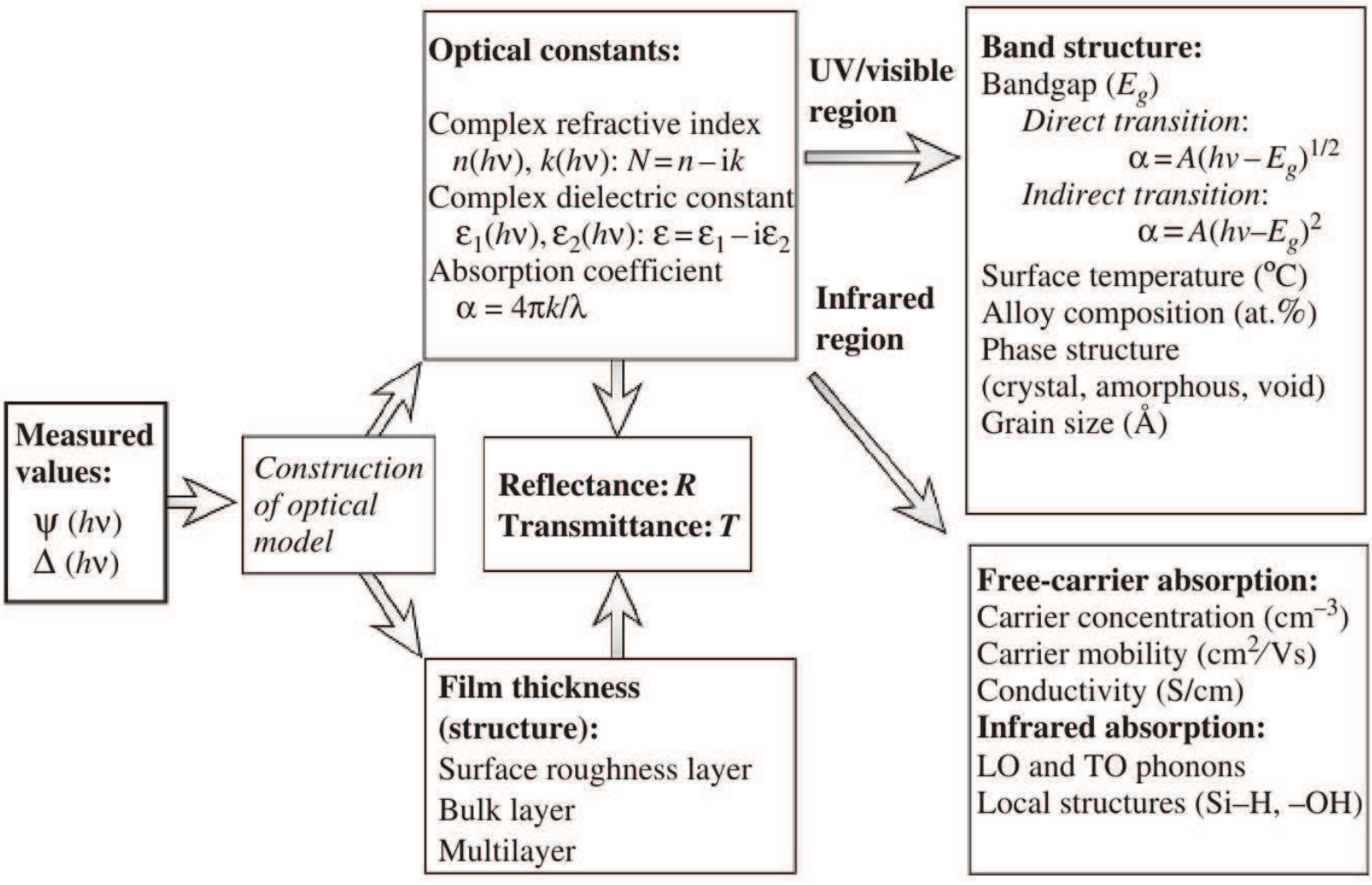
Optical constants:
Complex refractive index
n(hν), k(hν): N = n – ik
Complex dielectric constant
ε1(hν), ε2(hν): ε = ε1 – iε2
Absorption coefficient
α = 4πk/λ
UV/visible region
Infrared region
Band structure:
Bandgap (Eg)
Direct transition:
α = A(hν – Eg)1/2
Indirect transition:
α = A(hν–Eg)2
Surface temperature (°C)
Alloy composition (at.%)
Phase structure
(crystal, amorphous, void)
Grain size (Å)
Measured values:
ψ (hν)
Δ (hν)
Construction of optical model
Reflectance: R
Transmittance: T
Film thickness (structure):
Surface roughness layer
Bulk layer
Multilayer
Free-carrier absorption:
Carrier concentration (cm–3)
Carrier mobility (cm2/Vs)
Conductivity (S/cm)
Infrared absorption:
LO and TO phonons
Local structures (Si–H, –OH)

Figure

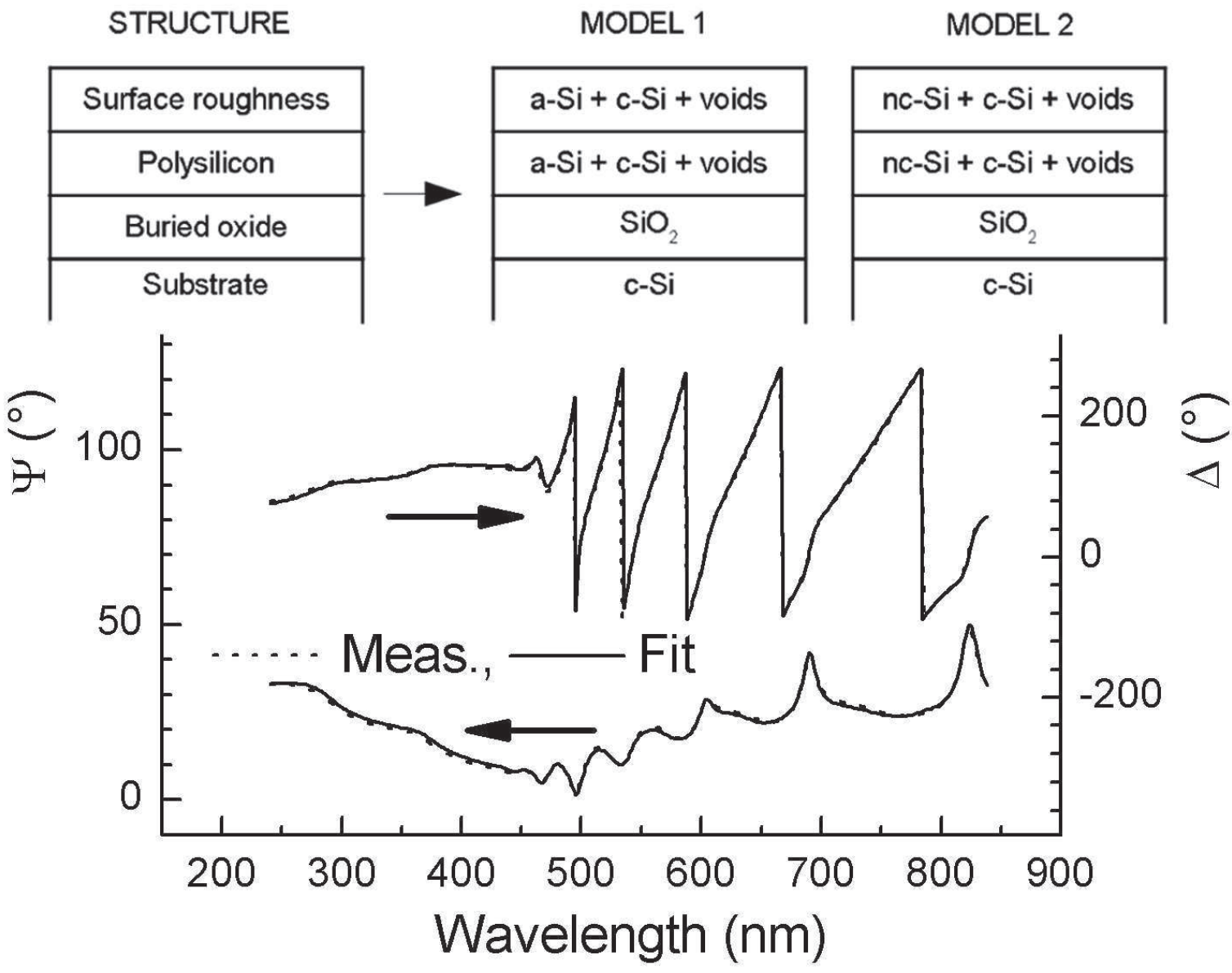
STRUCTURE
MODEL 1
MODEL 2
Surface roughness
Polysilicon
Buried oxide
Substrate
a-Si + c-Si + voids
a-Si + c-Si + voids
SiO2
c-Si
nc-Si + c-Si + voids
nc-Si + c-Si + voids
SiO2
c-Si
Ψ (°)
100
50
0
200
0
-200
Δ (°)
Meas., Fit
200
300
400
500
600
700
800
900
Wavelength (nm)

Figure

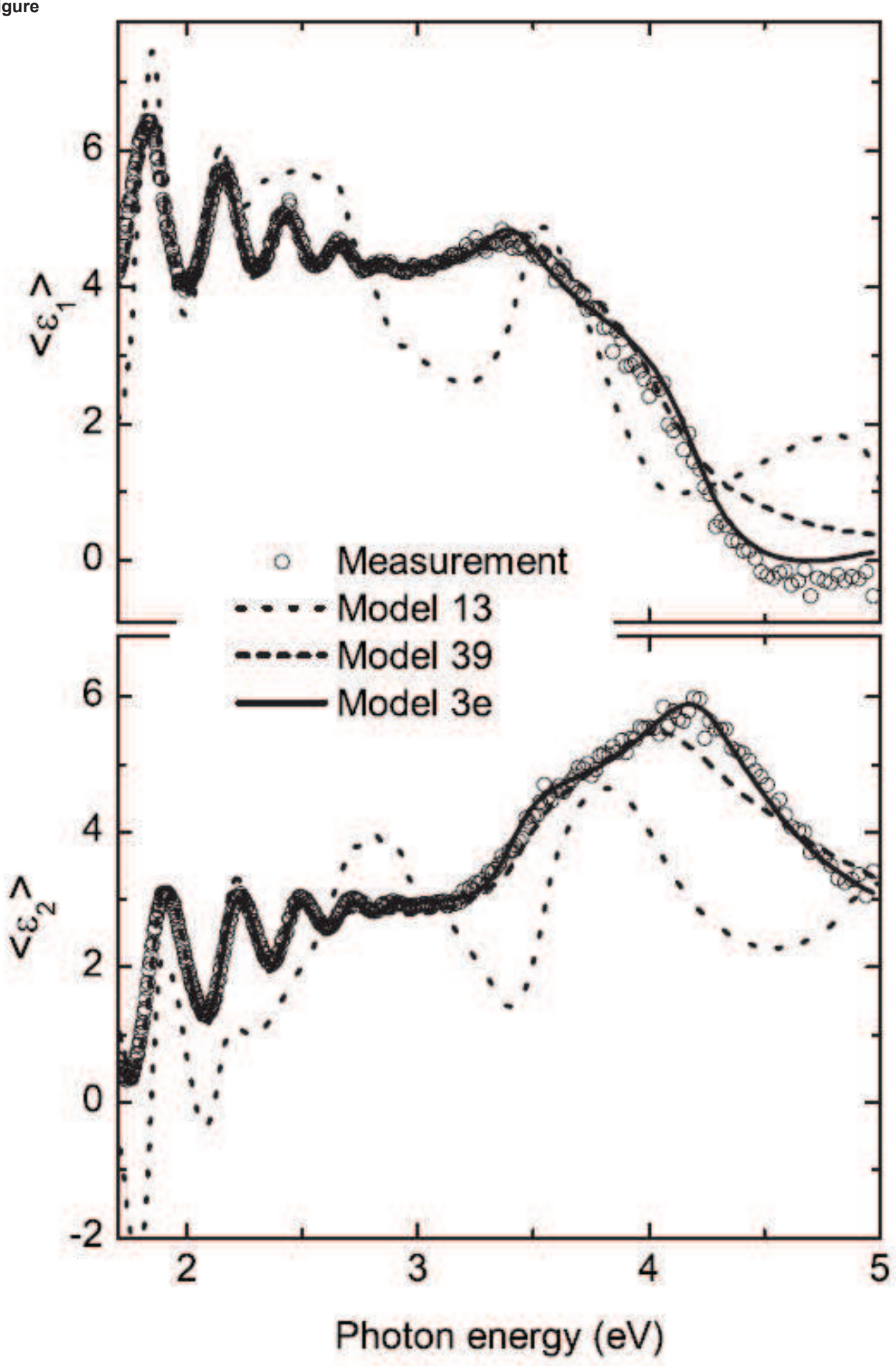
6
4
2
0
<ε1>
Measurement
Model 13
Model 39
Model 3e
6
4
2
0
-2
<ε2>
2
3
4
5
Photon energy (eV)

Figure

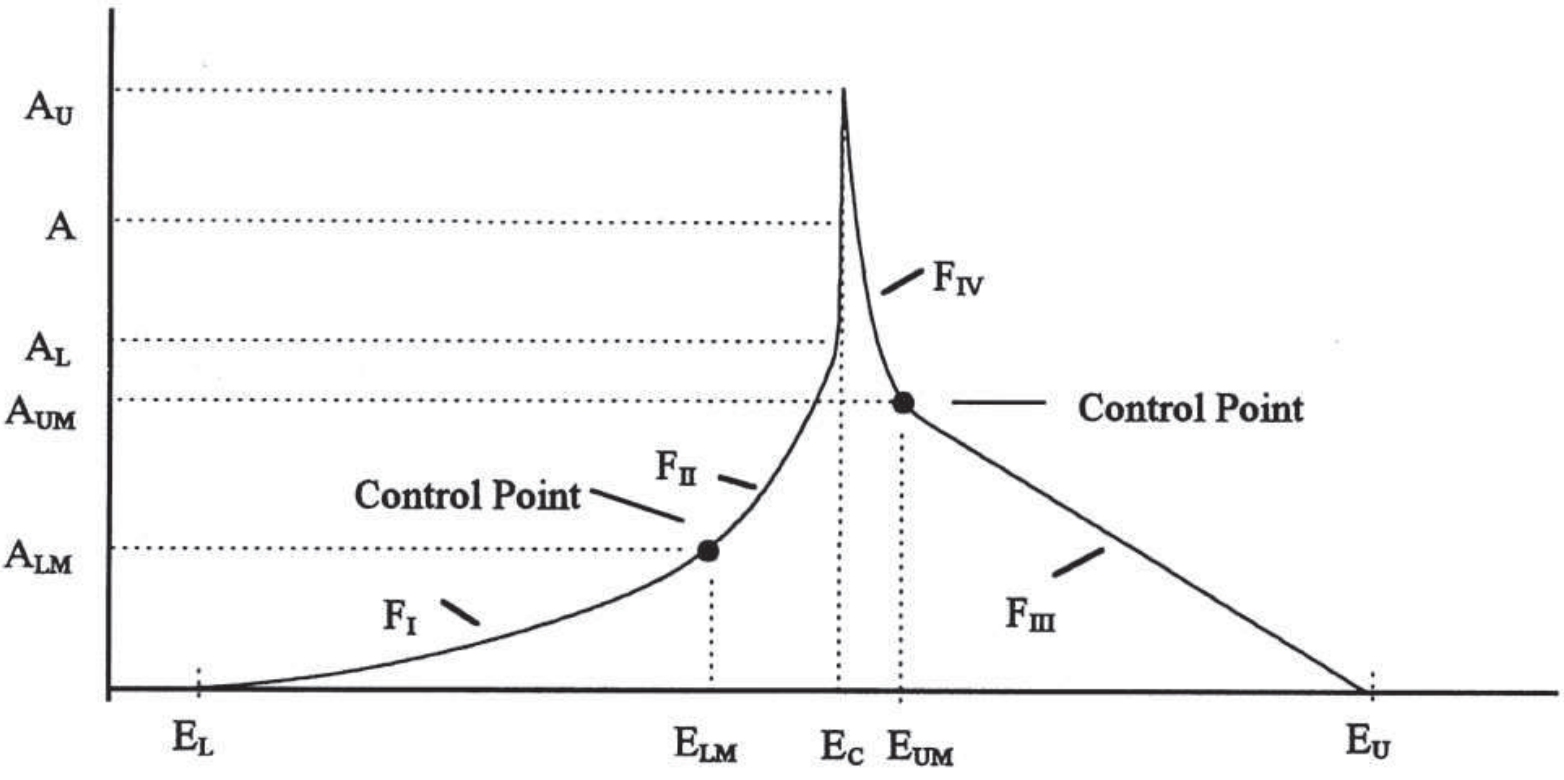
A_U
A
A_L
A_{UM}
A_{LM}
F_{IV}
Control Point
F_{II}
Control Point
F_I
F_{III}
E_L
E_{LM}
E_C
E_{UM}
E_U

Figure

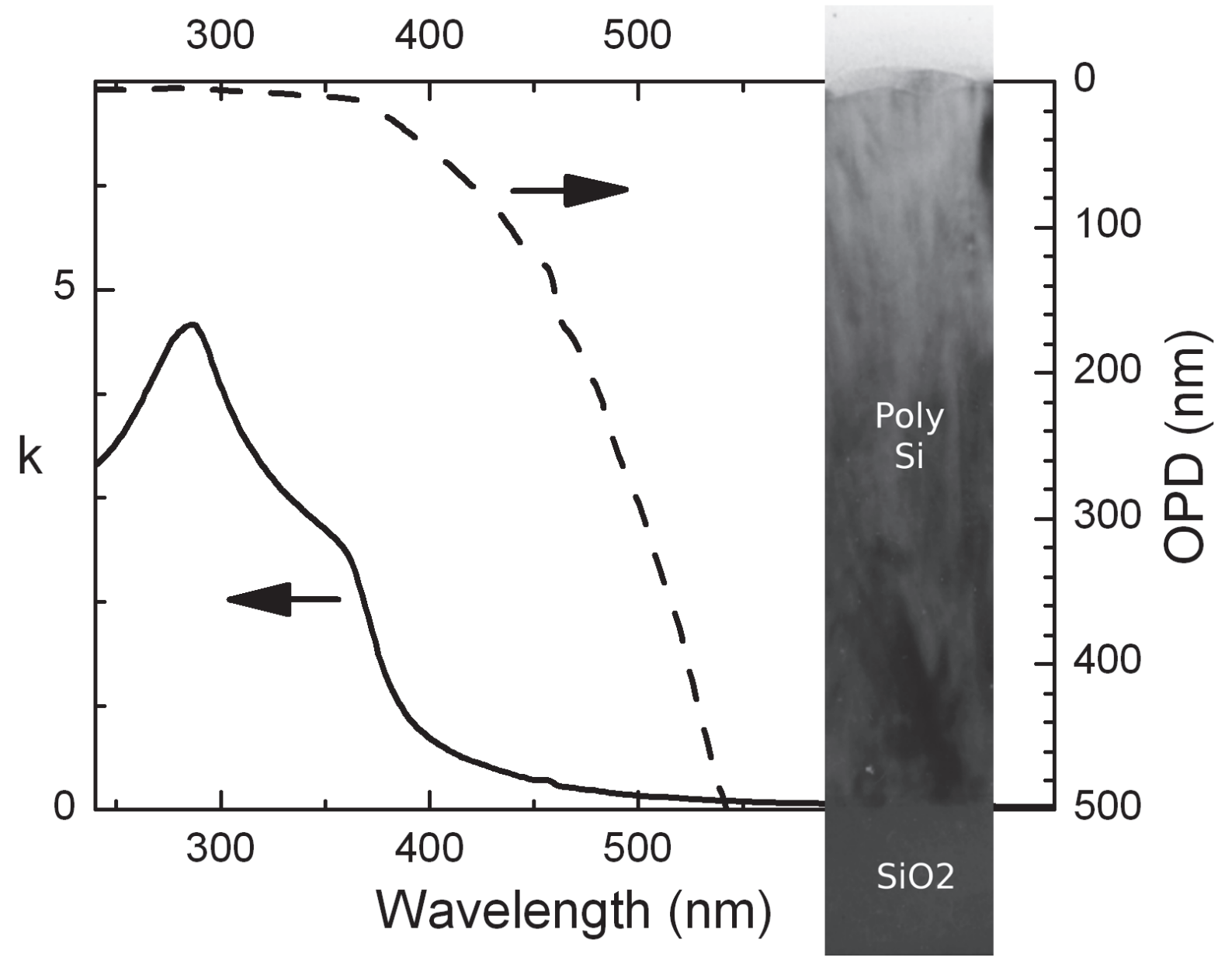
300
400
500
0
100
200
300
400
500
OPD (nm)
5
k
0
Poly
Si
SiO2
300
400
500
Wavelength (nm)

Figure

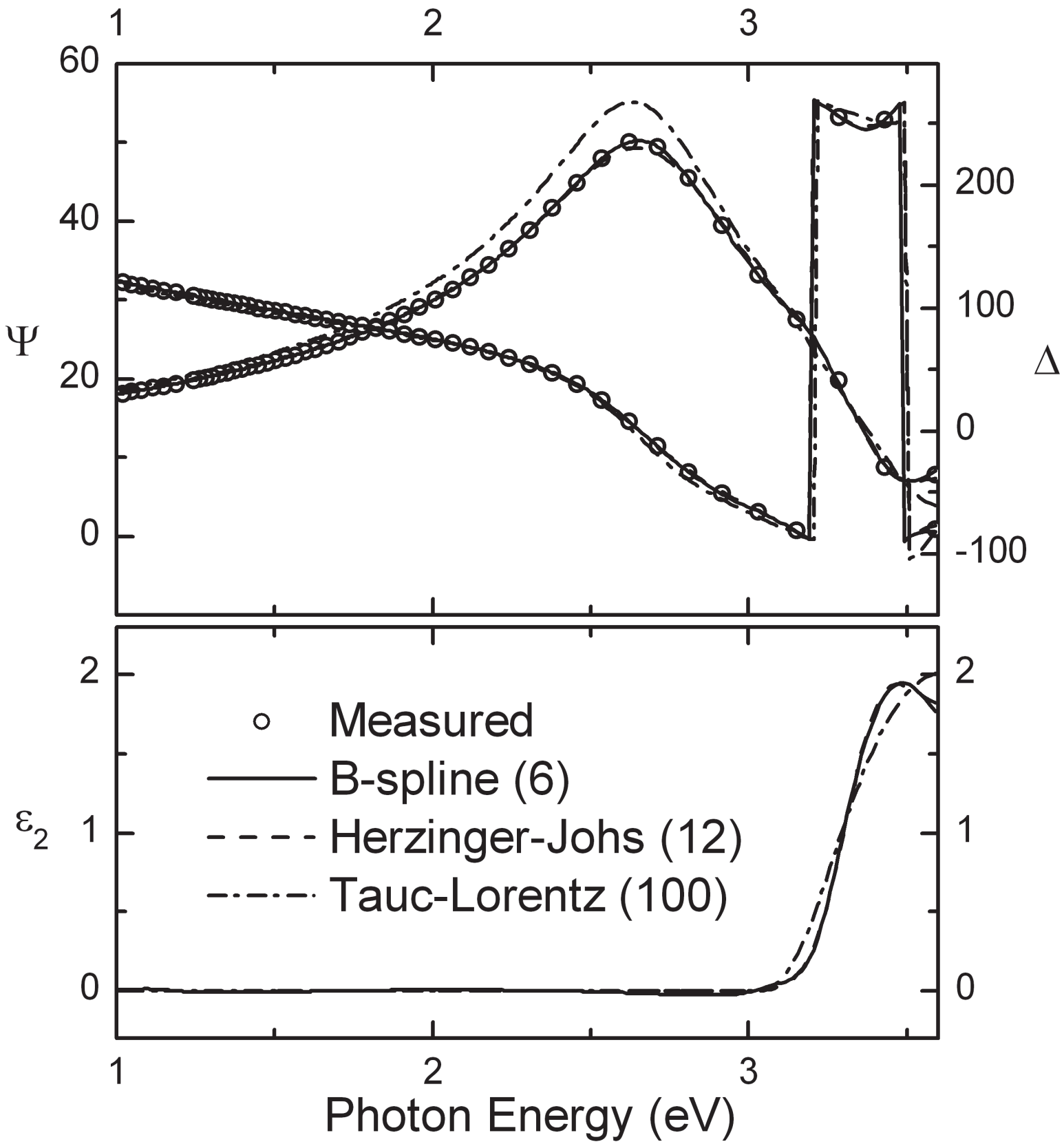
1
2
3
60
40
20
0
Ψ
200
100
0
-100
Δ
2
1
0
ε2
Measured
B-spline (6)
Herzinger-Johs (12)
Tauc-Lorentz (100)
Photon Energy (eV)